International Journal of Heat and Mass Transfer 52 (2009) 3305–3313

Contents lists available at ScienceDirect

International Journal of Heat and Mass Transfer

journal homepage: www.elsevier.com/locate/ijhmt

Evaporation rates of pure hydrocarbon liquids under the influences of natural convection and diffusion

Peter L. Kelly-Zion [a,*], Christopher J. Pursell [b], Ryan S. Booth [b], Alec N. VanTilburg [a]

[a] Engineering Science Department, Trinity University, San Antonio, TX 78212, USA
[b] Chemistry Department, Trinity University, San Antonio, TX 78212, USA

ARTICLE INFO

Article history:
Received 14 August 2008
Received in revised form 10 January 2009
Available online 19 March 2009

Keywords:
Evaporation
Natural convection
Buoyancy
Diffusion
Hydrocarbon

ABSTRACT

Evaporation of liquid hydrocarbons was studied in order to better understand the relative influences of diffusion and buoyancy-induced convection of the vapors on the evaporation rate. Evaporation rates were measured using a simple gravimetric technique and the behavior of the vapor layer that quickly forms above the film was observed using schlieren imaging. Even for conditions for which the influence of buoyancy is strong, the evaporation rates are well correlated by a one-dimensional diffusion model if an effective vapor layer thickness is used.

1. Introduction

In general, the rate at which a liquid evaporates is dependent on the transport of mass and energy occurring within both the liquid and vapor phases. Consequently, the general mathematical analysis of an evaporation problem involves coupled conservation equations for mass, momentum, and energy. These equations are difficult to solve analytically except for cases involving simplified geometry and/or limiting conditions for which one mode of transport dominates all others, for example when the evaporation is limited by the diffusion of vapor away from the liquid surface. In the past few decades, evaporation studies have concentrated on the cases of spherical droplets [1–13], liquid films or pools at the base of vertical columns (Stefan diffusion tube) [14–17], liquid films in convective environments [18–27], and droplets on heated surfaces [28–31]. Many aspects of liquid evaporation have been considered in these studies but few have focused on the relative effects of diffusion and buoyancy-induced (natural) convection in the vapor phase, which is the focus of this paper.

The effect of natural convection on the evaporation rate of a suspended spherical droplet was recently studied by Gogos et al. [1]. The authors' numerical analysis indicates that under normal gravity conditions, natural convection enhances evaporation. For the case of an *n*-heptane droplet in a nitrogen environment at high pressure and temperature, their numerical results show that buoyancy-induced motion causes the formation of a downward moving vapor plume to form. As the ambient pressure increases, the buoyancy-induced flow becomes stronger and increases the evaporation rate.

Two studies have looked at the effect of natural convection on the evaporation of liquid at the base of a vertical, open-ended tube (Stefan diffusion experiment). In the study by McBain et al. [14], the vapor produced by the evaporating liquid at the base of the tube is lighter than the ambient gas, thus promoting a convectively unstable situation, and the open end of the tube was exposed to a nominally quiescent atmosphere. Their numerical and experimental analyses indicate that for Grashof numbers less than 350, the vapor–gas mixture in the tube is essentially stagnant and evaporation is limited by the diffusion of vapors through the tube. As the Grashof number increases beyond 450, convective flow within the tube becomes increasingly stronger with a resulting increase in the evaporation rate. In contrast to the study of McBain et al., the numerical study of Markham and Rosenberger [15] considered the case in which the vapors produced by the evaporating film at the base of the cylinder are heavier than the ambient gas, which, assuming a one-dimensional system, is convectively stable. The boundary condition at the open end of the tube is zero vapor mass fraction, as would occur if a cross flow of ambient gas convects the vapors away. Despite the vapors being heavier than the ambient gas, the authors found that the no-slip boundary condition at the tube wall results in horizontal density gradients which, in turn, result in buoyancy-driven fluxes. This buoyancy effect was found to be very small and the total mass flux of the evaporating component was found to be essentially equal to the value computed according to the analytical solution for one-dimensional diffusion through a stagnant gas film, which is discussed in detail by Bird et al. [32].

* Corresponding author. Tel.: +1 210 999 7518; fax: +1 210 999 8037.
E-mail address: peter.kelly-zion@trinity.edu (P.L. Kelly-Zion).

0017-9310/$ - see front matter © 2009 Elsevier Ltd. All rights reserved.
doi:10.1016/j.ijheatmasstransfer.2009.01.015

Nomenclature

A	area of the liquid film (cm^2)
D	diffusion coefficient of vapor in air (cm^2/s)
E	evaporation rate (mg/s)
g	gravitational acceleration (m/s^2)
Gr	Grashof number
h	vapor diffusion distance (mm)
h_{eff}	effective vapor thickness (mm)
H	height of pedestal or depth of well (mm)
K	diffusion model constant (mm mg/s)
M	molar mass of vapor (g/mol)
M_a	molar mass of air (g/mol)
P	equilibrium vapor pressure (Torr)
P_{tot}	total ambient pressure (Torr)
R	universal gas constant (Torr cm^3/mol K)
R_d	radius of the disk on which the film is placed (cm)
T	film temperature (K)
Z	correction term for counter diffusion

Greek symbols

μ_a	absolute viscosity of the ambient air (Poise)
ρ_a	density of air (g/cm^3)
ρ_{mix}	density of vapor–air mixture (g/cm^3)

Subscripts

a	ambient air
d	disk on which the film is resides
eff	effective
tot	total

Experimental results of Beverly et al. [16,17] further validate the use of a one-dimensional diffusion model to compute the rate of evaporation through a vertical tube for cases in which the vapor is heavier than the ambient gas. In their experiments, a gas stream flowing in the longitudinal direction on the outside of the tube was used to establish the boundary condition at the top of the tube such that the rate of diffusion through the tube was set equal to the convective flow generated by the co-flowing stream at the top of the tube.

It is clear that a key to computing the evaporation rate is well-defined boundary conditions. For the case of evaporation into a quiescent environment, if the gravitational force is not important, then the vapor mass transfer problem may be modeled as diffusion into an infinite or semi-infinite region. For this case, the vapor continuously diffuses to further distances from the liquid surface. Thus the gradient in the vapor concentration and, therefore, the evaporation rate, continuously change. If, however, the gravitational force is significant then natural convection of the vapor–gas mixture can influence or even control the boundary condition. Because a mixed diffusion-natural convection boundary condition is difficult to determine analytically, there is a need for a simple model to compute the rates of evaporation for cases in which the evaporation rate is limited by the removal of the vapor from the liquid surface by such a mixed boundary condition (and not, for example, limited by the transport of thermal energy to the liquid surface).

For this study, gravimetric and optical measurements of the evaporation of liquid hydrocarbons in an initially quiescent atmosphere have been conducted in order to better understand the relative influences of vapor diffusion and buoyancy on the evaporation rate. A film on the order of 1 mm thick is generated by injecting the liquid onto a 13 mm diameter disk. Very quickly, a layer of vapor forms above the film. Since the vapor is heavier than the surrounding air, the tendency of the layer to grow vertically out from the film due to diffusion is constrained by a buoyancy force which acts to push the vapor layer down and radially outward. As a result, a vapor layer of nearly constant thickness is quickly established above the film. The effect of buoyancy-induced convection of the vapors on the evaporation rate of hydrocarbons having a wide range of volatilities was studied. As a means of varying the influence of buoyancy, the geometry surrounding the film was varied. Experiments were conducted with the film disk level with a surrounding horizontal surface, with the disk raised above the surface on a pedestal, and with the disk recessed below the horizontal surface in a cavity or well.

Evaporation rates were measured using a simple gravimetric technique. In addition, a schlieren imaging technique was used to provide estimates of the vapor layer thickness. For all measurements, evaporative cooling of the film was found to be negligible and, therefore, the evaporation rate was limited by the rate of removal of the vapor from the film surface.

The experiments clearly indicate that buoyancy has a strong influence on evaporation rate. Because buoyancy is influenced by geometry, the measured rates of evaporation were also dependent on geometry. However, for any given geometry, the rate of evaporation can be predicted with the use of a simple one-dimensional diffusion model if an effective value for the vapor layer thickness is used. The surprising result is that the same value for the effective vapor layer thickness may be used for all of the hydrocarbons that were studied.

2. Experimental

Evaporation rates were measured for eight hydrocarbon components, consisting of five alkanes from pentane to decane, two geometric isomers of hexane, cyclohexane and 3-methylpentane (3MP), and one isomer of octane, 2,2,4-trimethylpentane (isooctane). The isomers have equal molar masses and nearly equal heats of vaporization, but significantly different equilibrium vapor pressures. These components and their pertinent thermophysical properties are listed in Table 1. The volatilities of these components, as indicated by their equilibrium vapor pressures, vary by a factor of 400 and their molar masses vary by a factor of 2. All components are heavier than air, which has an average molar mass of approximately 29 g/mol.

Table 1 also contains computed Grashof numbers for the components studied. Since buoyancy-induced convection is driven by a difference in density and is resisted by viscosity, the Grashof number, Gr, may be used to indicate the potential strength of the convection. The Gr is computed according to Eq. (1), where ρ_{mix} and ρ_a are the densities of the vapor–air mixture above the film and of ambient air, μ_a is the absolute viscosity of the ambient air, R_d is a characteristic length, which is taken to be the radius of the disk on which the film resides, and g is the gravitational acceleration. The density of the mixture is computed assuming the partial pressure of the vapor is equal to the equilibrium vapor pressure, as may occur at the film surface. For the components used in this study, the Gr varies by a factor of 150. As shown in Table 1, pentane is the most volatile of the components and is expected to have the strongest convection, as indicated by Gr, despite having the lowest molar mass. This is because the equilibrium mole fraction of pentane in the mixture with air is high in comparison to the mole fractions of the other components, and therefore

Table 1
Thermophysical properties at 25 °C of the components studied. The vapor pressure values were obtained from [33]. Diffusion coefficient values are for vapor in air and were obtained from Beverley et al. and references therein [16] except for 3MP, which is assumed to be equal to hexane, and isooctane, which is assumed to be equal to octane. The mixture density was computed for a vapor–air mixture for which the partial pressure of the vapor is equal to the equilibrium vapor pressure. The total pressure was assumed to be 760 Torr.

Component	Vapor pressure (Torr)	Molar mass (g/mol)	Diffusion coefficient $\times 10^{-6}$ (m^2/s)	Grashof number *Gr*	Mixture density (mg/mL)
Pentane	513	72	8.4	11000	2.4
3MP	177	86	8.0	5400	1.8
Hexane	152	86	8.0	4300	1.7
Cyclohexane	98	84	7.3	2700	1.5
Isooctane	49	114	6.2	2200	1.4
Heptane	46	100	7.3	1600	1.4
Octane	14	114	6.2	600	1.2
Decane	1.3	142	5.7	70	1.2

the mixture density for pentane is high. For the same reason, decane is expected to have the weakest convection due to its low vapor pressure and the resulting low mole fraction in the mixture.

$$Gr = \frac{\rho_a(\rho_{mix} - \rho_a)R_d^3 g}{\mu_a^2} \quad (1)$$

To create the liquid film, a pipettor is used to deposit approximately 80 μl of liquid on a 13 mm diameter disk. The amount of liquid is sufficient to cover the whole top surface of the disk with liquid, but not so much that the liquid overflows the surface. The resulting film is anchored by surface tension along the edge of the disk. As a result of anchoring the film, the film's surface area remains approximately constant for the majority of its lifetime. As the film evaporates, eventually the film volume is insufficient to cover the surface and the film pulls free from the edge of the disk. All measurements were conducted prior to the time at which the film pulls from the edge of the disk.

The disk on which the film is deposited is made of zinc selenide. This material was selected in order to be compatible with a different experimental technique, which is not discussed here.

In order to control the relative influence of the buoyancy-induced convection, the geometry surrounding the film was varied, as depicted in Figs. 1–3. Experiments were conducted (i) with the disk nearly level with a surrounding horizontal circular surface (actually raised 0.4 mm above the surface), (ii) with the disk placed on a pedestal of height from 1.9 to 18.1 mm, and (iii) with the disk recessed below the horizontal surface in a well of depth from 1.5 to 39.7 mm. For good thermal contact, conductive grease was placed between the disk and the copper substrate. The diameter of the copper substrate is 44 mm. The temperature of the underside of the ZnSe disk and of the copper substrate at a location 1.5 mm below the disk were measured with thermocouples for the level and well geometries. During a test, the ZnSe temperature drops a small amount, up to 0.65 °C, and the temperature of the copper substrate drops even less. All experiments were contained in an isolated volume (ca. 6200 cm^3) to prevent drafts in the room from influencing the measurements. The ambient temperature and pressure were 25 °C and 1 atm.

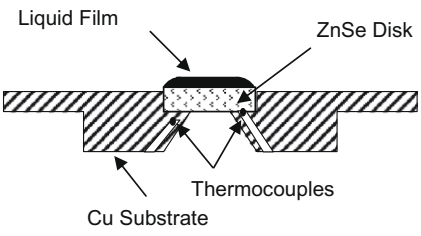

Fig. 1. Section view of the "level" geometry. The top surface of the ZnSe disk is 0.4 mm above the surface of the copper substrate and is 13 mm in diameter. The diameter of the copper substrate is 44 mm.

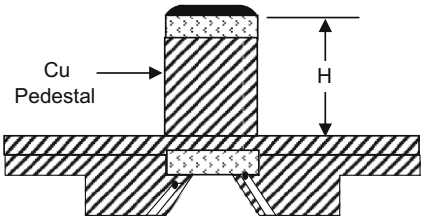

Fig. 2. Section view of a "pedestal" geometry. A copper cap is placed over the surface of the "level" geometry and a solid copper cylinder is used to raise the ZnSe disk above the substrate surface. Pedestals giving the following heights (H) were used: 1.9, 3.8, 5.9, 7.9, 11.9, and 18.1 mm.

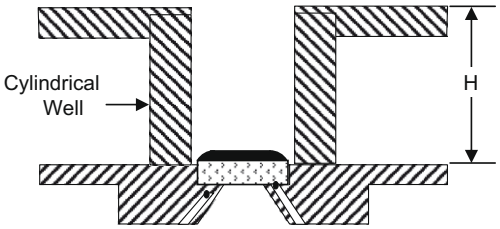

Fig. 3. Section view of a "well" geometry. A hollow cylinder of inner diameter 14 mm is placed around the ZnSe disk and a platform is placed at the top of the cylinder to duplicate the flat surface geometry of the substrate. Wells with the following depths (H) were used: 1.5, 5.9, 9.7, 14.7, 19.7, 29.8, 39.7 mm.

2.1. Schlieren method

Semi-quantitative measurements of the thickness of the vapor layer above a film were obtained using a schlieren imaging technique. This is a technique whereby the gradient in the refractive index may be measured optically and recorded using a digital camera. Light that passes through the vapor layer is bent at locations of non-zero gradient in the refractive index and results in changes in the image intensity of those locations. By placing a blade at the focal point of an imaging lens to block a portion of the undisturbed light, a gradient in the refractive index upstream of this lens causes light to be steered either away from or toward the blade and results in either more or less light passing the blade and consequently a brightening or darkening of the corresponding part of the image. However, only gradients normal to the edge of the blade are measured. Much more detail about this technique may be found in [34]. Images were recorded at a rate of 60 frames per second for up to 5 min so that changes in the behavior of the vapor layer over time could be observed.

Because the index of refraction is directly related to density, as given by the Gladstone–Dale Law, the schlieren technique is used to observe the vertical gradient in the vapor concentration. This gradient is high near the film surface and decreases in the vertical direction to zero. Where this gradient becomes zero is taken to be the vertical extent of a vapor layer that forms above the film since

beyond the vapor layer the gradient in concentration, as well as the magnitude of the concentration, must be zero. The location of this vapor boundary is affected by the sensitivity of the schlieren experiment, which is dependent primarily on two things, the amount of light blocked by the blade and the magnitude of the vapor index of refraction. Since the sensitivity of the experiments is not known, the results are considered semi-quantitative. Furthermore, because the indices of refraction differ for the components studied, the measured vapor layer thickness for one component cannot be compared quantitatively to that of another. Despite these limitations, the schlieren measurements provide very good qualitative insight into the nature of the vapor layer above the film.

2.2. Gravimetric method

Quantitative gravimetric measurements of the film evaporation were conducted using an analytical balance having a resolution of 0.1 mg. The balance was connected to a computer using the RS232 interface and mass data were collected at a rate of 10 Hz.

As shown in Fig. 4, the mass decreases at an approximately constant rate and therefore a linear fit was applied to the data in order to determine the evaporation rate, which equals the negative of the slope. Fig. 4 shows the evaporation of hexane for the level substrate geometry. The displayed linear trend is typical for all components and all geometries, with just the slope of the linear fit varying. At the beginning of a test, some of the mass data may be unstable due to an impulse generated by the momentum of the injected liquid. To prevent these unstable measurements from affecting the computed evaporation rate, the linear fit was applied to data starting at 90% of the initial mass. Although the evaporation rate is approximately constant, in some cases after about 50% of the film evaporates there is a perceptible reduction in the rate of evaporation, which is due to the reduced surface area of the film. Therefore, the data range for the linear fit is limited to mass greater than 50% of the initial mass.

At least three measurements were conducted for each condition. For all gravimetric tests the experiment-to-experiment variation is less than 5% and typical values are approximately 2%.

3. Results and discussion

3.1. Schlieren images

The schlieren images clearly indicate the strong influence that buoyancy-induced convection has on the transport of the vapors. Figs. 5–7 show the vapor layers (actually, the vertical concentration gradients) that develop over hexane films for three geometries. In each of these figures, the vapor layer is the dark cloud that resides above the substrate, which is also dark but is separated from the vapor cloud by a bright line, which is a result of the diffraction of light at the surface of the substrate. For a given geometry, the shape of the vapor layer is quickly established and stays approximately constant until the film pulls from the edge of the disk as the last portion of the liquid film evaporates.

Fig. 5 shows the evaporation of a hexane film from the level geometry. Diffusion of vapor up and away from the film is constrained by gravity, which pushes the vapor cloud down and causes a buoyancy-induced convective flow radially outward. The vapor layer is approximately constant over most of the surface of the substrate. At the left and right sides of the figure, the vapors can be seen "pouring" over the edge of the substrate. This flow is even more apparent in videos.

As the film is raised above the substrate surface, as shown in Fig. 6 for the 7.9 mm pedestal height, the horizontal surface of the substrate becomes less of an impediment to the buoyancy-induced flow and convection of the vapors away from the film surface increases. Fig. 6 shows vapors flowing off of the film surface, collecting on the horizontal surface of the substrate, and then flowing over the edge of the substrate. A schlieren video of this phenomenon for the case of an 11.9 mm tall pedestal may be viewed from the online version of this paper.

Within the confines of a cylindrical well, buoyancy cannot convect the vapors away from the film. (As mentioned previously, the results of Markham and Rosenberger [15] suggest there may be a negligible convective flow.) This case is shown in Fig. 7, where the vapors escaping from the top of a 9.7 mm deep well may be

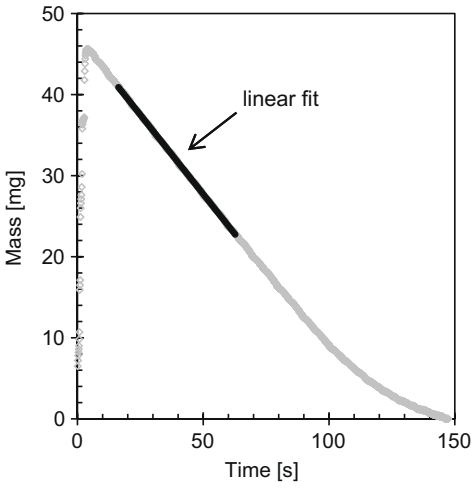

Fig. 4. Gravimetric data for the evaporation of hexane from the level geometry at 25 °C. A line is fit to the data over the range from 90% to 50% of the initial mass. The evaporation rate is taken to be the negative of the slope of the line.

Fig. 5. Schlieren image of the vapor layer above an evaporating hexane film from the level substrate geometry. The liquid film is outlined by the white lines.

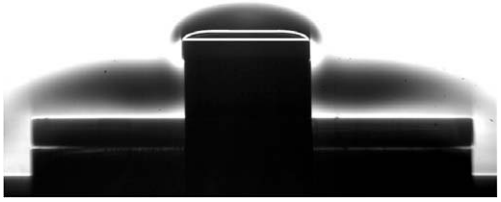

Fig. 6. Schlieren image of the vapor layer above an evaporating hexane film on top of a pedestal of height 7.9 mm. The liquid film is outlined by the white lines. (A schlieren video of this phenomenon for the case of an 11.9 mm tall pedestal may be viewed from the online version of this paper.)

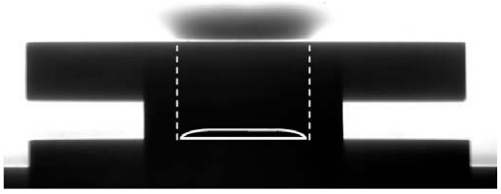

Fig. 7. Schlieren image of the vapor layer above an evaporating hexane film within a well of depth 9.7 mm. The white dashed lines outline the interior of the well and the white solid lines outline the liquid film.

seen. Relative to the level and pedestal geometries, the well geometry results in a much smaller vapor cloud.

It is interesting to compare the shape of the vapor cloud at the top edge of the well (Fig. 7) to that at the edge of the film in the pedestal geometry (Fig. 6). For the well geometry, the visible boundary of the vapor cloud extends up and radially out from the top of the well, suggesting that the rate of vertical diffusion is of the same order of magnitude as the radial mass transfer, which is likely a combination of diffusion and buoyancy-induced convection. In contrast, the shape of the vapor cloud at the edge of the film in the pedestal geometry extends downward which suggests that buoyancy-induced convection is controlling the flow of the vapor. Since both images are of hexane evaporation, the difference in the strength of the buoyancy-induced convection for the two cases cannot be explained by a difference in molar mass. Instead, the difference in vapor–air mixture density likely explains the difference in the strength of buoyancy. Because the well confines the vapor in a column above the film, it creates a large resistance for the transport of vapor away from the evaporating film and results in a slow evaporation rate and a low vapor mole fraction within the vapor cloud at the top of the well compared to that in the cloud above the film in the pedestal geometry.

As a means of studying further the effect of buoyancy on the vapor layer, a series of schlieren images was taken of pentane, hexane and octane films for various geometries. For each image, the vapor layer thickness was measured above the center of the film. For the level and pedestal geometries, the vapor layer thickness was measured from the surface of the film to the top edge of the vapor layer, whereas for the well geometries the vapor layer thickness was measured from the top of the well to the top edge of the vapor layer. In this way, the vapor layer thickness measured for a well geometry is comparable to that measured for the level geometry since the substrate geometry at the exit of the well is analogous to the geometry of the level. The results are plotted in Fig. 8. In this figure, well depth decreases from left to right on the abscissa, as if well depth were a negative pedestal height. Only hexane vapor thickness was measured for the well geometries whereas vapor thickness was measured for all three components for the level and pedestal geometries. Recall that due to differences in measurement sensitivities for the three components, the vapor thickness values may not be compared from one component to another, though for each component the values are comparable from one geometry to another. Furthermore, the given values should be considered semi-quantitative because of the unknown sensitivity of the measurement. Actual vapor layer thicknesses may be greater than the measured values, but not lower.

As shown in Fig. 8, the vapor layer thickness is strongly dependent on the substrate geometry. The hexane vapor thickness is zero (immeasurable) above the 29.8 mm well and increases as the well depth decreases. In going from the level geometry to pedestal geometries of increasing height, the vapor thickness decreases until a critical height is attained beyond which the vapor thickness becomes insensitive to the pedestal height. The horizontal surface of the substrate catches the vapor that flows off of the film and a relatively thick cloud develops over the substrate that impedes the flow. The thick cloud over the substrate may be seen in Fig. 6. As the pedestal height increases, eventually the film is raised above this cloud. It is believed that when the film is above the cloud, the cloud no longer impedes the vapor flow off of the film and the thickness of the vapor layer above the film becomes insensitive to pedestal height. The case shown in Fig. 6 is a hexane film on a 7.9 mm high pedestal, which is above the minimum height needed for the vapor layer thickness to be insensitive to pedestal height.

In comparing the trends of vapor layer thickness versus pedestal height for the three components, it appears that thickness quickly drops to a constant value for pentane and hexane while the reduction is more gradual for octane. The critical height above which the vapor layer thickness remains constant is approximately 2 mm for pentane, between 2 and 4 mm for hexane, and between 4 and 6 mm for octane. Though pentane is the lightest of the three, the vapor–air mixture density of the pentane cloud above the substrate may be greater than that of the hexane or octane cloud due to its higher vapor mole fraction, which results from pentane's faster evaporation rate. As discussed previously, it is the difference in density between the mixture and air that is believed to induce the flow and thus a stronger flow in the case of pentane ($Gr = 11000$) may cause a thinner cloud above the substrate than occurs in the cases of hexane ($Gr = 4300$) and octane ($Gr = 600$). As a consequence of the thinner cloud above the substrate, the thickness of the vapor layer over the film becomes independent at a shorter pedestal height for pentane.

3.2. Gravimetric results

In an attempt to sort out the relative effects of diffusion and buoyancy-induced convection on the evaporation rate, gravimetric experiments were conducted with the well geometry, for which

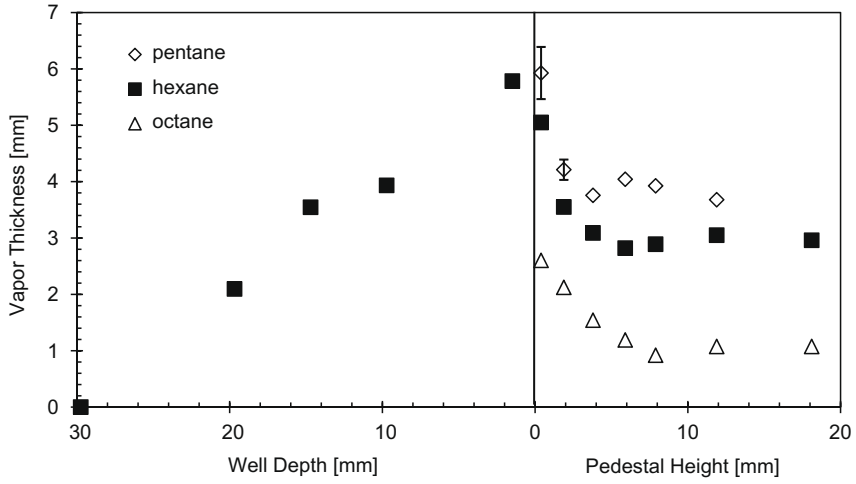

Fig. 8. Vapor layer thickness estimated from the schlieren images of pentane, hexane and octane evaporating from the different geometries. The vapor layer thickness for pentane and octane are given for the level and pedestal geometries while the vapor layer thickness for hexane includes the well geometries in addition to the level and pedestal geometries. Error bars are smaller than the data symbols except where displayed.

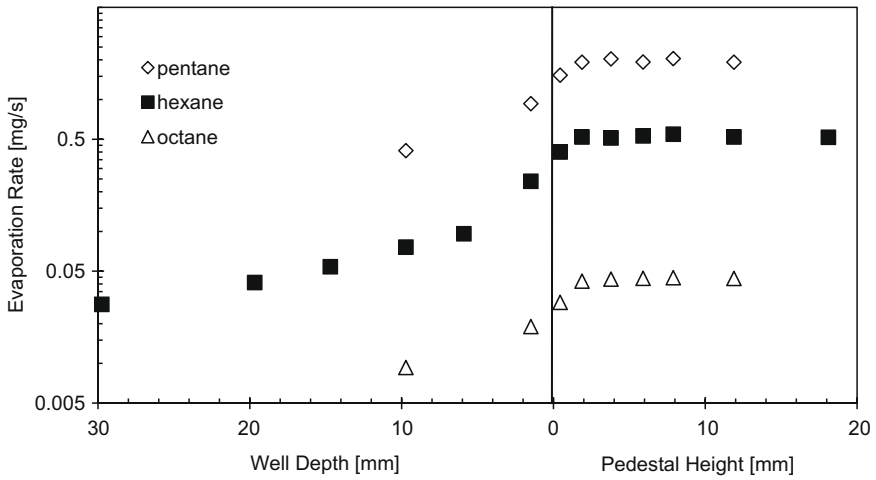

Fig. 9. Measured evaporation rates of pentane, hexane and octane evaporating from the different geometries. Note that the evaporation rate is given on a logarithmic scale in order to accommodate the wide range of rates. Just two well geometries were tested for pentane and octane films. Error bars are smaller than the data symbols.

diffusion is expected to control the evaporation rate, with the pedestal geometry, for which the schlieren images suggest that convection is enhanced if not dominant, and for the level geometry. Fig. 9 presents measured evaporation rates for pentane, hexane, and octane for the three geometries. The evaporation rates are plotted on a logarithmic scale in order to accommodate the large difference in rates between pentane and octane. The figure shows that a component's evaporation rate increases as the well depth decreases, the rate increases further in going from a shallow well to the level geometry, and it continues to increase as the film is raised up to the 1.9 mm pedestal. For pedestal heights taller than 1.9 mm, a component's evaporation rate remains constant.

We focus first on the results of the well experiments, for which diffusion is expected to control the evaporation rate. Fig. 10 shows the measured evaporation rates of a hexane film in wells of depths from 9.7 to 39.7 mm. The evaporation rate is linear with respect to the inverse of the well depth, as would be expected if the rate is controlled by one-dimensional diffusion. Eq. (2) is the equation for steady-state one-dimensional diffusion through a tube [35].

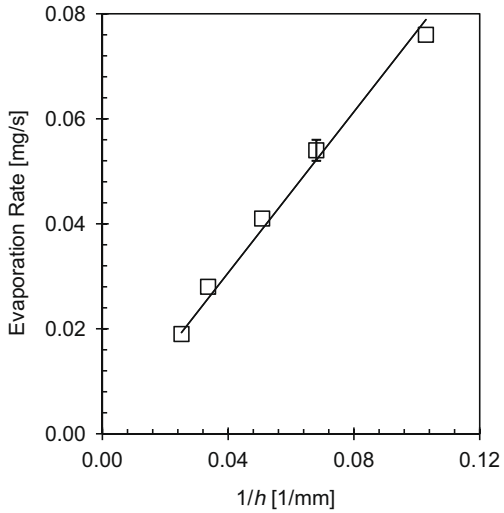

Fig. 10. Measured evaporation rates for hexane in wells of depths from 9.7 to 39.7 mm. The linear relationship between the evaporation rate and the inverse of the well depth provides support for a one-dimensional diffusion model as given in Eq. (2). Error bars are smaller than the data symbols except where displayed.

In this equation, E is the evaporation rate, M is the molar mass, A is the surface area of the film, P is the equilibrium vapor pressure, D is the diffusion coefficient of the vapor in air, z is a correction term that accounts for the counter diffusion of the air and is given in Eq. (3) [36], R is the universal gas constant, and T is the film temperature. h is the distance through which the vapor diffuses and is set equal to the well depth. As a means of writing the equation in a more compact form, K is used to group all of the terms except the diffusion distance, h, on the right hand side of Eq. (2). The counter-diffusion correction factor, z, is dependent only on P and the ambient pressure, P_{tot}.

$$E = \frac{MAPDz}{RTh} = K/h \tag{2}$$

$$z = \left(\frac{P_{tot}}{P}\right)\ln\left[\frac{1}{(1 - P/P_{tot})}\right] \tag{3}$$

While Fig. 10 indicates that the evaporation rate is linearly related to the inverse of the well depth, as suggested by Eq. (2), Figs. 7 and 8 demonstrate that a thin vapor layer exists at the top of the well and thus the vapor concentration is non-zero there. Schlieren images indicate that the vapor layer thickness at the top of the well decreases with increasing well depth, as the evaporation rate decreases. For the results presented in Fig. 10, it appears that above the exit of the well, the removal of the vapor is quick compared to the rate of diffusion through the well and thus the well depth accurately determines the evaporation rate. Using Eq. (2), h may be computed from the measured evaporation rates ($h = K/E$) and the results are all within 3% of the well depths.

Evaporation rates measured in shallow wells of depths of 1.5 and 5.9 mm do not follow the trend with inverse well depth, presumably because the rate of vapor removal at the exit of the well is of the same order of magnitude as the rate of diffusive transport of vapor through the well. The measured evaporation rates of these two short wells are lower than what would be predicted by the linear trend shown in Fig. 10. This result suggests that vapor diffusion plays a significant role in the transport of vapors from the exits of these two well geometries, in effect increasing the distance through which the vapor must diffuse. Using Eq. (2) to compute h from the measured evaporation rates, values of 3.9 mm and 8.4 mm are obtained for the well depths of 1.5 mm and 5.7 mm, respectively.

For the deeper well geometries, it is readily understandable that the distance through which vapor diffusion is occurring is approx-

imately equal to the depth of the well. In order to investigate the significance of diffusion for the level and pedestal geometries, for which a diffusive length scale is unknown, the measured evaporation rates were plotted as a function of K. This plot is shown in Fig. 11 and contains data for all of the components for the level geometry (which is actually raised 0.4 mm), the 1.9 mm pedestal, and the 1.5 mm well, and for all components except decane for the 11.9 mm pedestal and 9.7 mm well. The surprising result is that the measured evaporation rates for each of the five geometries are linear with respect to K, and not just for the 9.7 mm well. The evaporation rates from the level and pedestal geometries, despite qualitative evidence from the schlieren images of significant buoyancy-induced convection, are well correlated by the one-dimensional diffusion equation. Referring to Eq. (2), one can see that an effective diffusion thickness, h_{eff}, may be defined as the inverse of the slope of the linear fits. This effective thickness is constant for a given geometry and, therefore, is independent of the physical properties of the evaporating component. Furthermore, the relationship between E and K for the 1.9 and 11.9 mm pedestals are essentially the same, indicating that the evaporation rates of all of the measured components become constant for pedestals of heights equal to or taller than 1.9 mm.

In comparing the evaporation rates in Fig. 9 to the vapor layer thickness values in Fig. 8, one can see that for pentane the evaporation rate and the vapor thickness plateau at about the same pedestal height. However, for hexane and octane the vapor layer thickness plateaus at a taller pedestal height than does the evaporation rate. Thus there is not a direct relationship between the evaporation rate and the vapor layer thickness for the pedestal geometries. For the conditions of these experiments, the evaporation rate is limited by the removal of vapor from the surface of the film and therefore is determined by the rates of diffusion and buoyancy-induced convection. The relative strengths of these transport mechanisms determine the vapor layer thickness, as diffusion tends to transport vapor along the vertical concentration gradient (as well as the radial gradient), causing an increase in the vapor layer thickness, whereas convection tends to transport the vapor radially over the film and thereby reduce the vapor layer thickness. The fact that the evaporation rate remains constant as the vapor layer thickness decreases with increasing pedestal height beyond 1.9 mm suggests that the magnitudes of the rates of vapor removal by diffusion and convection are approximately equal. Thus, as convection becomes more prominent as the film is raised above the vapor cloud that collects over the surface of the substrate, the evaporation rate remains unchanged.

To investigate further this trade-off between convection and diffusion, the evaporation rate was plotted as a function of Gr for five geometries and is presented in Fig. 12. Although there is not an analytical expression for the dependence of the evaporation rate on Gr, this parameter is commonly used in numerical and empirical analyses involving natural convection, e.g. [14]. Fig. 12 indicates that for the geometries studied, the relationship between the evaporation rate and Gr is linear, with the exception of the highest Gr, which corresponds to pentane. Ignoring pentane for the moment, the fact that the evaporation rate is proportional to Gr, even for the 9.7 mm well geometry for which convection is expected to be negligible, is surprising. Furthermore, considering Figs. 11 and 12, one can see that the evaporation rate of any of the geometries may be considered to be proportional either to K, which indicates the strength of diffusion for a given geometry, or Gr, which indicates a potential for buoyancy-induced convection.

The fact that either K or Gr may be used to correlate the evaporation rate suggests the rate of diffusion and the strength of convection are both strongly influenced by the same physical properties. What drives the convection is the difference in densities between the vapor–air mixture and the surrounding air. Using the mixture at the surface of the film as the representative vapor–air density, this density difference is directly proportional to the product of the equilibrium vapor pressure and the molar mass (assuming a mixture of ideal gases). As shown in Eqs. (2) and (3), the one-dimensional diffusion model also is dependent on the equilibrium vapor pressure and molar mass, and for components for which the counterdiffusion correction factor, z, approximately equals one the rate of diffusion is directly related to the product of vapor pressure and molar mass. All of the components in this study have a value of z between 1.00 and 1.15, except for pentane, which has a value of 1.67.

The relationship between the driving force for buoyancy-induced convection, Gr, and the rate of one-dimensional diffusion through a given length, K, is plotted in Fig. 13. As may be seen in the figure, the relationship between Gr and K is reasonably linear when pentane is excluded from the correlation. This linear relationship may explain why for any given geometry the evaporation rates of components having a wide variety of properties may be computed either with a simple one-dimensional diffusion model or with a linear correlation with Gr. For example, while convection

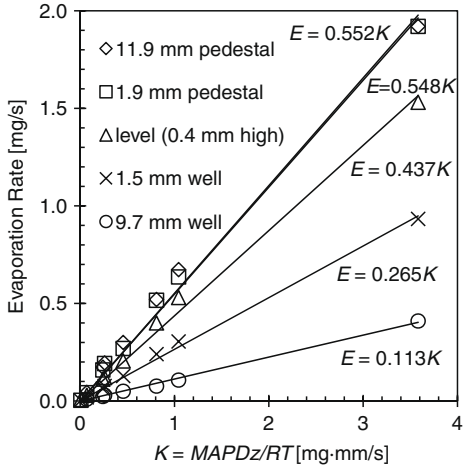

Fig. 11. Measured evaporation rates plotted as a function of the mathematical form of the steady-state, one-dimensional diffusion equation, K. Slopes of the linear fits represent $1/h_{eff}$. Note that the linear fits for the two pedestal geometries are essentially equal.

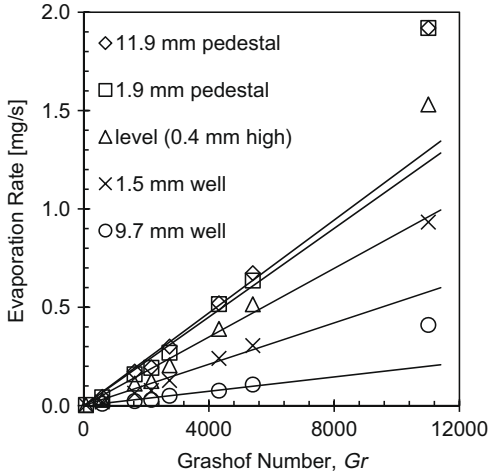

Fig. 12. Measured evaporation rates plotted as a function of the Grashof number, Gr, for five geometries. For each geometry, and for all of the components except pentane (Gr = 11000) the relationship between evaporation rate and Gr is linear.

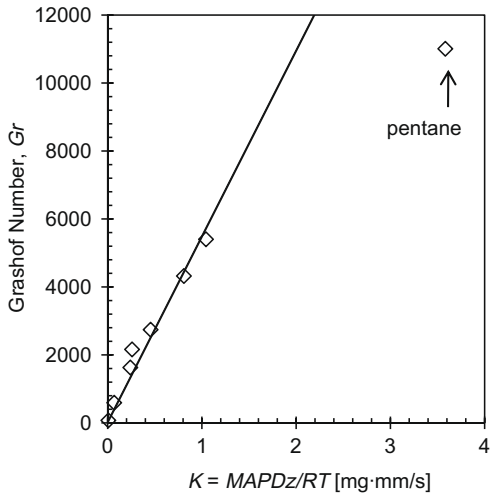

Fig. 13. A plot of the Grashof number, which is indicative of the strength of the buoyancy-induced convection, as a function of *K*, which is indicative of the rate of diffusion through a given length. The solid line is a linear fit to the values of all of the components except pentane, for which *z* deviates significantly from one.

may play a major role in removing vapors from above a hexane film on a pedestal, convection is unlikely to play a significant role for an octane film on the same pedestal due to the very small difference in densities between the vapor–air mixture and the surrounding air. Although the relative importance of diffusion and convection to the evaporation rate may differ for hexane and octane, since both transport mechanisms depend strongly on the product of the vapor pressure and the molar mass, the evaporation rate is well correlated either to *K* or *Gr* for both components.

As shown in Fig. 13, pentane does not fall on the line relating *Gr* and *K*. The cause of this discrepancy is pentane's high *z* value, which results in the one-dimensional diffusion model, Eq. (2), not being directly proportional to the equilibrium vapor pressure. According to the diffusion model, evaporation increases with *z*. The fact that the measured pentane evaporation is greater than the linear correlation with *Gr* may indicate that diffusion plays an appreciable role in transporting vapors from the surface of the pentane film, even for a tall pedestal geometry. Since the buoyancy-induced convection is expected to be most prominent for pentane, then if diffusion has an appreciable influence on the evaporation rate for pentane films, diffusion very likely has an appreciable influence for all of the components.

As discussed previously, the schlieren images clearly show vapors flowing off of the pedestal films. It may be that a sublayer, for example a boundary layer, exists where diffusion is dominant over convection. The effective vapor layer thickness, h_{eff}, which is defined by the correlations in Fig. 11, may be equal to, or at least related to, the thickness of this diffusive sublayer. In all cases, the computed effective vapor layer thickness is less than the estimated vapor layer thickness based on the schlieren images.

4. Conclusions

Schlieren imaging and gravimetric methods were used to study the rates of evaporation of a series of eight hydrocarbons having equilibrium vapor pressures that vary by a factor of nearly 400 and molar masses that vary by a factor of 2. Experiments were conducted for a range of geometries to vary the relative influences of diffusion and convection on the evaporation rate. Schlieren images clearly indicate that buoyancy-induced convection can have a strong influence on the vapor layer that forms above the film for the level and pedestal geometries, whereas diffusion appears to be the dominant transport mechanism for a film contained in a deep well. Those geometries that enable convection (level and pedestal) result in significantly faster evaporation rates than do the well geometries.

Despite the influence of buoyancy, it was shown that a simple steady-state, one-dimensional diffusion model can be used to calculate evaporation rates for all components when an effective vapor layer thickness value, which is dependent only on the substrate geometry, is used. It was also shown that the evaporation rates for all of the components except pentane are proportional to *Gr*, which is used as an indicator of the potential for convection. The applicability of the two models is reconciled by the fact that both are strongly influenced by the product of the equilibrium vapor pressure and the molar mass. The evaporation results for pentane, which has a large counterdiffusion correction factor, suggest that even for conditions for which a strong convective flow is apparent, diffusion contributes to the vapor transport, perhaps due to the existence of a diffusive sublayer.

The main conclusions are summarized in the following list.

- The substrate geometry has a significant effect on the evaporation rate. Geometries that enable buoyancy-induced convection result in faster evaporation rates than do geometries for which diffusion dominates.
- For a given substrate geometry, the shape of the vapor layer is quickly established and stays approximately constant.
- The shape and thickness of the vapor layer varies for the different geometries, presumably due to the varying influence of buoyancy-induced convection.
- The shape of the vapor layer above the well geometry suggests that vertical diffusion of the vapor is of the same magnitude as the radial transport of vapor by convection and diffusion.
- Comparing the shape of the vapor layer for a film on a pedestal to the vapor layer over the well suggests that buoyancy-induced convection has a relatively strong influence on the vapor layer for a pedestal geometry.
- As pedestal height increases, the evaporation rate increases until a height is reached beyond which the evaporation rate no longer changes.
- The evaporation rates measured for the well geometries vary with well depth and can be modeled with a simple steady-state, one-dimensional diffusion model where the diffusion height is defined as the geometrical well depth.
- Even for geometries for which convection is significant, the one-dimensional diffusion model may be used to compute the evaporation rate if an effective vapor layer thickness is introduced. The effective vapor layer thickness is dependent on the geometry and is independent of the film component.
- With the exception of pentane, the evaporation rates of all components are proportional to *Gr* for all geometries, including those for which diffusion dominates.
- Diffusion and convection are both strongly dependent on the product of the equilibrium vapor pressure and the molar mass.
- Even for the conditions for which convection is strongest, diffusion appears to play an appreciable role in determining the evaporation rate.
- The existence of a diffusive sublayer, e.g. a boundary layer, is hypothesized.

Acknowledgments

We are grateful for the assistance of the following students: Will French, Derek Rose, Alejandro Rodriguez, and Brian Malpede. Acknowledgement is made to the Donors of the American Chemical Society Petroleum Research Fund for partial support of this

work. Acknowledgement is also given to the National Science Foundation for partial support of this work.

Appendix A. Supplementary data

Supplementary data associated with this article can be found, in the online version, at doi:10.1016/j.ijheatmasstransfer.2009.01.015.

References

[1] G. Gogos, S. Soh, D.N. Pope, Effects of gravity and ambient pressure on liquid fuel droplet evaporation, Int. J. Heat Mass Transfer 46 (2) (2003) 283–296.
[2] H. Jia, G. Gogos, High pressure droplet vaporization; effects of liquid-phase gas solubility, Int. J. Heat Mass Transfer 36 (18) (1993) 4419–4431.
[3] R. Kneer, M. Schneider, B. Noll, S. Wittig, Diffusion controlled evaporation of a multicomponent droplet: theoretical studies on the importance of variable liquid properties, Int. J. Heat Mass Transfer 36 (9) (1993) 2403–2415.
[4] C.M. Megaridis, W.A. Sirignano, Multicomponent droplet vaporization in a laminar convective environment, Combust. Sci. Technol. 87 (1–6) (1992) 27–44.
[5] W.A. Sirignano, Fuel droplet vaporization and spray combustion theory, Prog. Energy Combust. Sci. 9 (4) (1983) 291–322.
[6] C.K. Law, Recent advances in droplet vaporization and combustion, Prog. Energy Combust. Sci. 8 (3) (1982) 171–201.
[7] C.K. Law, Multicomponent droplet combustion with rapid internal mixing, Combust. Flame 26 (2) (1976) 219–233.
[8] S. Zhang, G. Gogos, Film evaporation of a spherical droplet over a hot surface: fluid mechanics and heat/mass transfer analysis, J. Fluid Mech. 222 (1991) 543–563.
[9] G. Chen, S.K. Aggarwal, T.A. Jackson, G.L. Switzer, Experimental study of pure and multicomponent fuel droplet evaporation in a heated air flow, Atomization Sprays 7 (3) (1997) 317–337.
[10] A.K. Ray, J. Lee, H.L. Tilley, Direct measurements of evaporation rates of single droplets at large Knudsen numbers, Langmuir 4 (3) (1988) 631–637.
[11] K. Harstad, J. Bellan, Modeling evaporation of Jet A, JP-7, and RP-1 drops at 1 and 15 bars, Combust. Flame 137 (1–2) (2004) 163–177.
[12] R.J. Hopkins, J.P. Reid, A comparative study of the mass and heat transfer dynamics of evaporating ethanol/water, methanol/water, and 1-propanol/water aerosol droplets, J. Phys. Chem. B 110 (7) (2006) 3239–3249.
[13] R.L. Matlosz, S. Leipziger, T.P. Torda, Investigation of liquid drop evaporation in a high temperature and high pressure environment, Int. J. Heat Mass Transfer 15 (4) (1972) 831–852.
[14] G.D. McBain, H. Suehrcke, J.A. Harris, Evaporation from an open cylinder, Int. J. Heat Mass Transfer 43 (12) (2000) 2117–2128.
[15] B.L. Markham, F. Rosenberger, Velocity and concentration distribution in a Stefan diffusion tube, Chem. Eng. Commun. 5 (5–6) (1980) 287–298.
[16] K.J. Beverley, J.H. Clint, P.D.I. Fletcher, Evaporation rates of pure liquids measured using a gravimetric technique, Phys. Chem. Chem. Phys. 1 (1) (1999) 149–153.
[17] K.J. Beverley, J.H. Clint, P.D.I. Fletcher, Evaporation rates of structured and non-structured liquid mixtures, Phys. Chem. Chem. Phys. 2 (18) (2000) 4173–4177.
[18] I.N. Tsimpanogiannis, Y.C. Yortsos, A.K. Stubos, Evaporation of a stagnant liquid, Ind. Eng. Chem. Res. 39 (5) (2000) 1505–1513.
[19] M.T. Pauken, An experimental investigation of combined turbulent free and forced evaporation, Exp. Therm. Fluid Sci. 18 (4) (1999) 334–340.
[20] W.-M. Yan, C.-Y. Soong, Convective heat and mass transfer along an inclined heated plate with film evaporation, Int. J. Heat Mass Transfer 38 (7) (1995) 1261–1269.
[21] J. Himmelsbach, B. Noll, S. Wittig, Experimental and numerical studies of evaporating wavy fuel films in turbulent air flow, Int. J. Heat Mass Transfer 37 (8) (1994) 1217–1226.
[22] P.W.M. Brighton, Evaporation from a plane liquid surface into a turbulent boundary layer, J. Fluid Mech. 159 (1985) 323–345.
[23] M. Gerendas, W. Wittig, Experimental and numerical investigation on the evaporation of shear-driven multicomponent liquid wall films, J. Eng. Gas Turb. Power 123 (3) (2001) 580–588.
[24] J.W. Palen, Q. Wang, J.C. Chen, Falling film evaporation of binary mixtures, AIChE J. 40 (2) (1994) 207–214.
[25] P.W.M. Brighton, Further verification of a theory for mass and heat transfer from evaporating pools, J. Hazard. Mater. 23 (2) (1990) 215–234.
[26] R. Chebbi, S.E.M. Hamam, M.K.M. Al-Kubaisi, K.M. Al-Jaja, S.A.M. Al-Shamaa, Evaporation of complex and pure components liquid hydrocarbon mixtures, J. Chem. Eng. Jpn. 36 (12) (2003) 1510–1515.
[27] Z.R. Regnier, B.F. Scott, Evaporation rates of oil components, Environ. Sci. Technol. 9 (5) (1975) 469–472.
[28] E.F. Crafton, W.Z. Black, Heat transfer and evaporation rates of small liquid droplets on heated horizontal surfaces, Int. J. Heat Mass Transfer 47 (6) (2004) 1187–1200.
[29] J.-H. Kim, S.I. Ahn, J.H. Kim, W.-C. Zin, Evaporation of water droplets on polymer surfaces, Langmuir 23 (11) (2007) 6163–6169.
[30] D. Fardad, N. Ladommatos, Evaporation of hydrocarbon compounds, including gasoline and diesel fuel, on heated metal surfaces, Proc. Inst. Mech. Eng. – D J. Automobile Eng. 213 (6) (1999) 625–645.
[31] K.S. Birdi, D.T. Vu, A. Winter, A study of the evaporation rates of small water drops placed on a solid surface, J. Phys. Chem. 93 (9) (1989) 3702–3703.
[32] R.B. Bird, W.E. Stewart, E.N. Lightfoot, Transport Phenomena, John Wiley & Sons, New York, 1960. pp. 522–527.
[33] C.L. Yaws, Thermodynamic and Physical Property Data, Gulf Publishing Company, Houston, 1992.
[34] G.S. Settles, Schlieren and Shadowgraph Techniques, Springer-Verlag, Berlin, 2006.
[35] F.P. Incropera, D.P. DeWitt, Fundamentals of Heat and Mass Transfer, second ed., John Wiley & Sons, New York, 2002. pp. 884–886.
[36] W. Jost, Diffusion in Solids Liquids and Gases, Academic Press, New York, 1952. p. 9.